

## Article

# Numerical Analysis of Concentrated Solar Heaters for Segmented Heat Accumulators

Martin Beer , Radim Rybár, Jana Rybárová, Andrea Seňová \*  and Vojtech Ferencz

Institute of Earth Sources, Faculty of Mining, Ecology, Process Technologies and Geotechnology, Technical University of Košice, Letná 9, 042 00 Košice, Slovakia; martin.beer@tuke.sk (M.B.); radim.rybar@tuke.sk (R.R.); jana.rybarova@tuke.sk (J.R.); vojtech.ferencz@tuke.sk (V.F.)

\* Correspondence: andrea.senova@tuke.sk

**Abstract:** This presented paper focuses on the design and evaluation of the concept of concentrated solar heaters for segmental heat accumulators, which are designed to cover the energy needs of selected communities in terms of food preparation without the need for fossil fuels, which have a negative impact not only on the climate but especially on health. The proposed device is based on the traditional method of food preparation in the so-called earth oven; however, the fire-heated stones are replaced with heat accumulators heated by solar radiation. This approach eliminates the need to change common and long-term habits of food preparation for selected communities. The device connects solar vacuum heat pipes, a solar radiation concentrator, and heat accumulators. The concept was evaluated based on computational fluid dynamics (CFD) analysis with the use of a transient simulation of selected operating situations in three geographical locations. The results showed a significant temperature increase of the heat accumulators, where in the most effective case the temperature increased up to 227.23 °C. The concept was also evaluated based on a calorimetric analysis of the system consisting of heat accumulators and food. The resulting temperature in the considered case reached the pasteurization temperature necessary for safe and healthy food preparation.



**Citation:** Beer, M.; Rybár, R.; Rybárová, J.; Seňová, A.; Ferencz, V. Numerical Analysis of Concentrated Solar Heaters for Segmented Heat Accumulators. *Energies* **2021**, *14*, 4350. <https://doi.org/10.3390/en14144350>

Academic Editor: Carlo Renno

Received: 22 June 2021  
Accepted: 15 July 2021  
Published: 19 July 2021

**Publisher's Note:** MDPI stays neutral with regard to jurisdictional claims in published maps and institutional affiliations.



**Copyright:** © 2021 by the authors. Licensee MDPI, Basel, Switzerland. This article is an open access article distributed under the terms and conditions of the Creative Commons Attribution (CC BY) license (<https://creativecommons.org/licenses/by/4.0/>).

**Keywords:** solar energy; solar oven; concentrating; CFD analysis

## 1. Introduction

One of the most significant characteristics of the last decade is the fight against climate change, the negative impact of which is gradually manifested in a whole range of natural as well as human processes and phenomena [1–5]. Consumption of primary energy sources on a global scale is constantly growing [6–9]; over the last decade it is possible to record an increase of 14.6% [10]. However, this growth is uneven from a global perspective, with many developed countries in Western Europe and North America showing stagnation or even decline in this parameter for a long time. The increase in consumption is mainly due to the region of Africa, the Middle East, and Southeast Asia [11]. When studying the projections for the consumption of primary energy sources for the coming decades, it is clear that the gap between developed and developing countries will increase.

With current trends, the so-called developing countries will account for 67% of total energy consumption in 2040 [12], which is mainly covered by fossil fuels, the extraction, processing and use of which have many negative effects [13,14]. In developing countries, this increase is caused by the rapid growth of the population, which puts pressure on the provision of basic energy needs in the housing sector, i.e., especially cooking, heating, and preparation of hot water.

In developing countries, food preparation is largely covered using coal, solid biomass, and only to a lesser extent are gaseous fuels used in the form of propane-butane [15,16]. According to a study [17] about 3 billion people use for food preparation the so-called open fire, which burns solid biomass or coal. Depending on the country, in addition to coal, a whole range of solid biomass is used as an energy carrier, starting with animal

excrement, wood biomass, or waste from wood processing activities [18]. The use of solid biomass brings several negative factors [19–21]. The most fundamental is the extensive use of forests beyond their sustainability. The second, no less serious, is the impact of imperfect combustion and particulate matter on human health [22–25]. This impact is multiplied by the fact that there are mainly women and small children in the vicinity of the open fire, for whom solid pollutants or increased CO<sub>2</sub> levels are more significant threats. According to a study [26], 1 million people, mainly women and children, lose their lives each year because of the safety and health impacts of open fires.

The availability of energy as well as the reduction of negative environmental impacts in the food preparation process is currently addressed by many technologies [27–32]. Among the simplest and most promising is the use of solar energy. It is mainly the use of concentration technology, increasing the power input from solar radiation, the overall efficiency, and thus also the resulting temperatures influencing the time or ability to prepare food. According to Solar Cookers International, more than 4 million solar cookers of various technologies are currently used by more than 11 million people [33]. Solar cookers can be divided into three main categories: solar box/panel cookers, parabolic solar cookers, and evacuated tube solar cookers [34]. The principle of operation of the first category is based on the capture of solar radiation in a thermally insulated box, the inner walls of which show a high degree of reflectivity of solar radiation. This guarantees an increase in the temperature throughout the inner volume, allowing the preparation of food, which, however, usually takes a longer period of time compared to other methods.

By contrast, parabolic solar cookers use a reflective-concentration element (dish), which concentrates sunlight into a small space and thus ensures the achievement of high temperatures and the speed of food preparation. The most effective way of using solar energy for food preparation is the use of evacuated tube solar cookers, where food is placed in a thermally insulated glass vacuum tube, which is in the focal point of the concentrating device. This method is comparable in time and temperature to the preparation of food on gas cookers, but the disadvantage is the space limitation given by the diameter of the tube. Another way to increase the thermal efficiency of solar cookers is to implement heat accumulators into their construction. Solar Cookers are prominently represented in the field of scientific research, and efforts to increase the efficiency of existing installations can be observed, as well as proposals for new technical solutions for solar cookers.

Morales et al. [35] designed a multifunctional solar system, consisting of two modules for food preparation and water heating. The design combines the features of a solar radiation collector that utilizes a revolving compound parabolic concentrator and channel. In the presented tests, the solar cooker part of the device achieved a heat output of 150 W. Zafar et al. [36] presented a new design of a solar cooker using the upper, lower, and front reflective surface. In the experiment, the new device reached a temperature of 100 °C–135 °C in 1 to 1.5 h. Ayub et al. [37] focused on increasing the power of a solar cooker. The authors supplemented the solar oven with a heat accumulator based on metal hydride. The results of the numerical analysis confirmed the expected increase in the energy efficiency of the modified solar oven from 6% to 42%.

Bhave and Kale [38] have developed a solar cooker with a heat accumulation function for high-temperature applications. A eutectic mixture of sodium nitrate and potassium nitrate was used as a heat accumulator, allowing the authors to reach a cooking temperature of 170 °C–180 °C. Kumaresan et al. [39] proposed a flat plate cooking unit for an indirect mode of solar cooking, using heat accumulation via phase change material (PCM) from the sugar alcohol group D-Mannitol. A numerical assessment of the operation showed an increase in the efficiency of the flat plate cooking unit to 41%. A change in the internal arrangement of the solar cooker was discussed by Sagade et al. [40]. The authors proposed a transparent modification of the top cover of the interior space intended for food preparation, which increased the heat flow directly into the prepared food and thus the total preparation temperature at the level of 120 °C–130 °C.

Mawire et al. [41], in their work, compared two devices designed for cooking using solar radiation. Both devices used heat accumulation usable at a time of lower solar radiation intensity. Sunflower oil and erythritol have been used as a heat accumulator. In terms of the use of accumulated energy, the authors confirmed greater efficiency in favor of erythritol. Chaudhary and Yadav [42] proposed a device enabling the simultaneous preparation of two separate meals, using a vacuum tube collector, which heats heat transfer medium and subsequently two in-series connected vessels containing the prepared food. The presented simultaneous operation increases the usability of the solar cooker in terms of repeated cooking during the day, as well as cooking over a longer period. Hosseinzadeh et al. [43] described a solar cooker consisting of a vacuum tube in which a steel vessel is placed for preparing food or heating water. The heat flow was increased by the concentration of solar energy using parabolic concentration equipment. However, for this type of device, the limiting element is the diameter of the vacuum tube, which limits the volume as well as the dimensions of the prepared dish.

This presented paper deals with the design and evaluation of an innovative technical design of cooking with the use of solar energy. The essential feature is the connection of the solar vacuum tube collector, the concentrating device, and the heat accumulation element. The resulting device, by changing the concept, solves two problems of solar cookers using vacuum tube-limited capacity of the space for food preparation and the need to change traditional cooking procedures. The proposed concept implements modern technologies into centuries-old methods of food preparation, which can increase the acceptance of the device in selected communities for everyday use. The innovativeness of the proposed device lies in the use of heat accumulators, which are heated by solar radiation in proposed device. The heated heat accumulators are then used outside the body of the solar heater for food preparation, heating, or disinfection of water. Verification of the function and evaluation in terms of the achieved parameters was performed through numerical CFD analysis.

## 2. Materials and Methods

### 2.1. Concentrated Solar Heater for Segmental Heat Accumulators

The technical solution concerns a solar heater designed for heating heat accumulators for their further use mainly for the heat treatment of food (meals) in the so-called earth oven. The method of preparing food in the earth oven consists of placing the food and a source of heat (most often fire-heated stones) in the prepared pit and its subsequent covering. The slowly released heat, thanks to thermal insulation in the form of soil, will then heat-treat the desired food.

The proposed device eliminates the need for a fire while using solar radiation to heat the heat accumulators, which replace the stones heated by fire. The solar heater of heat accumulators is intended primarily for use in warmer climatic zones with predominantly sunny weather, in regions with a low standard of living, or low availability of fuels or other heat sources. The proposed solar heater consists of three main (1–3) and four supporting parts (4–7), which are shown in the partial section view in Figure 1. The functional part of the design consists of the double-layered solar vacuum glass tube with open endings and without selective coating, in which heat accumulators made of cast iron are located. In the gap between the layers of glass is a secured vacuum, which increases the thermal resistance of the tube and thus improves its thermal insulation properties.

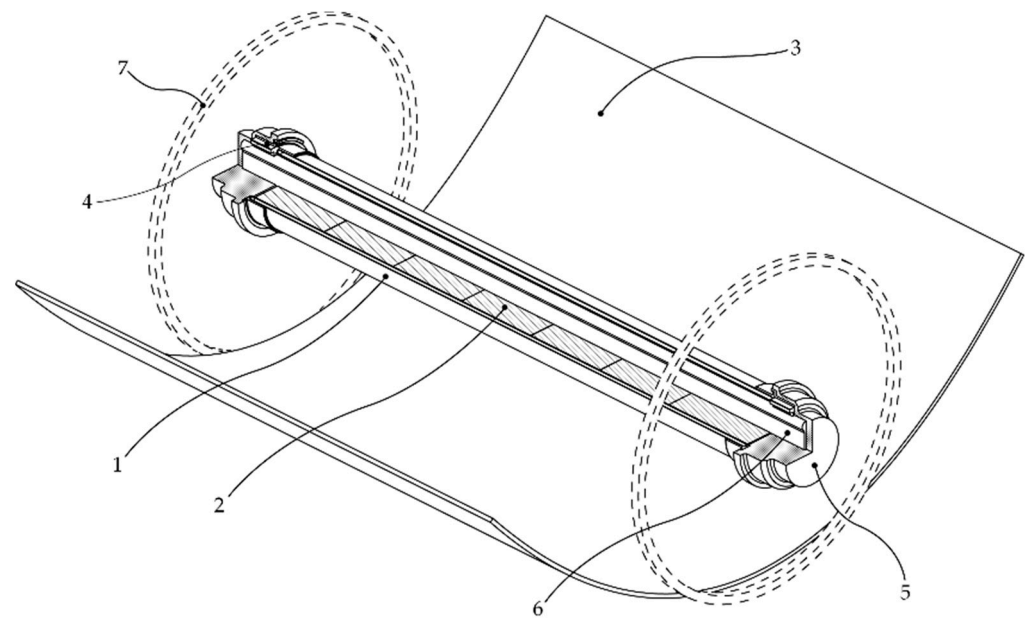


**Figure 1.** Concentrated solar heater for segmental heat accumulators (1—double-layered solar vacuum tube, 2—heat accumulator, 3—solar radiation parabolic concentrator, 4—heat accumulator support system, 5—thermal insulation block, 6—central beam, 7—chassis (not part of the design).

Solar radiation is focused by means of a concentration device attached to the chassis and wheels, respectively, which, however, are not essential from the point of view of the heat accumulation function and have therefore not been detailed in this phase of the design. The sides of the vacuum tube, the supporting system, and the heat storage elements are covered by a heat insulation block eliminating heat losses.

The heat accumulators are slid onto a beam which is self-supporting, attached to the hubs of the chassis and the glass tube, as shown in Figure 2. Thanks to this solution, the heat accumulators do not directly load the glass vacuum tube with their weight and the position of their center of gravity is still at one point, which is achieved by the independent mounting of the central beam with respect to the chassis hubs.

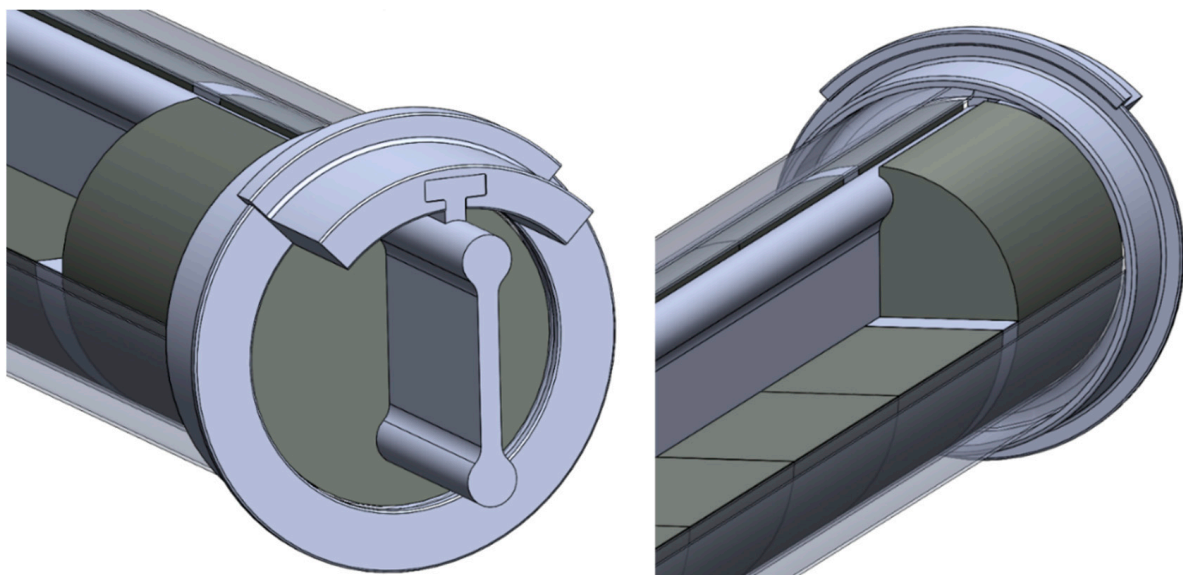


**Figure 2.** Detailed view of the 3D model of the supporting system of the heat accumulators.

Due to the technical and operational properties of the vacuum tube, it is advantageous that the concentrated solar heater of segmental heat accumulators can also be used to store heat accumulators in a charged state for their later use (for the time without sufficient solar radiation). Another advantageous fact is that the absorption surface where the photothermal conversion takes place is the surface of the segmental heat accumulators themselves, and not the inner surface of the glass tube as is the case with conventional solar vacuum collector designs, which helps with the heat transfer process. It is also positive that the vacuum tube of a transparent heating chamber allows for a visual inspection of the heating process of the individual segmental heat accumulators, which can be provided with a temperature indicator for this purpose. From the point of view of service life, it is advantageous that segment heat accumulators, unlike PCM and other heat accumulators, have an unlimited service life and a high resistance to damage.

Positioning the concentrator in the required position relative to the transparent heating chamber, depending on the position of the sun, is manual, by simultaneously turning both support wheels of the chassis. The working position of the solar heater with respect to the direction of incidence of solar radiation, during its operation, is such that the longitudinal axis of the horizontally placed heating chamber is at a right angle to the direction of incidence of the sun's rays. The basic principle of the proposed solar concentrated device is depicted in Figure 3.

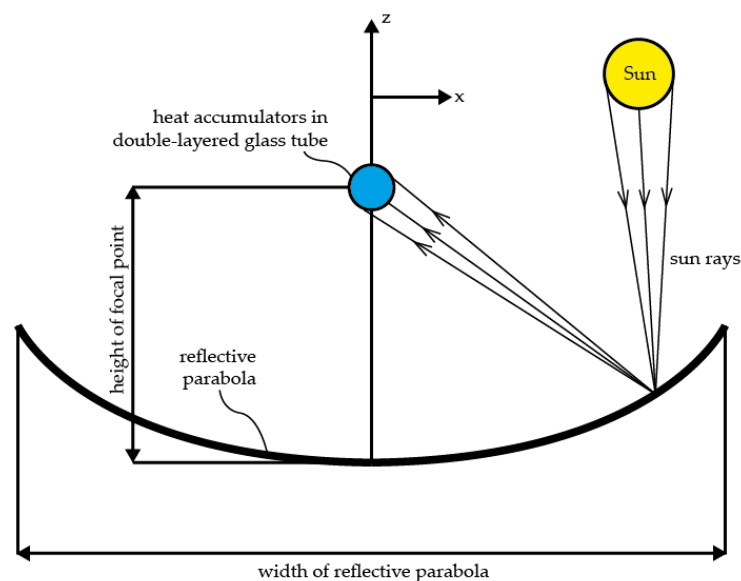


**Figure 3.** Basic principle of the proposed concentrated solar device.

## 2.2. Methodology

The concept of the concentrated solar heater of segmental heat accumulators was evaluated from the point of view of achieving selected values of operating parameters: average and daily temperature course of the heat accumulator temperature and the average temperature of the solar glass vacuum tube. The proposed design was assessed through numerical CFD analysis, which saves time, costs, working material, and with which the authors have many years of experience [44]. The analyzed geometry was simplified by eliminating the support system and chassis, which do not occur in the process of heat accumulation. Thus, only the concentration-reflective element, the glass vacuum tube, the heat accumulators, and the thermal insulation blocks closing the openings of the vacuum tube were featured in the simulations. This simplification has resulted in a significant reduction in the demands on the computing apparatus and hence the computing time. Figure 4 shows the basic layout, boundary conditions, and description of the calculation model.

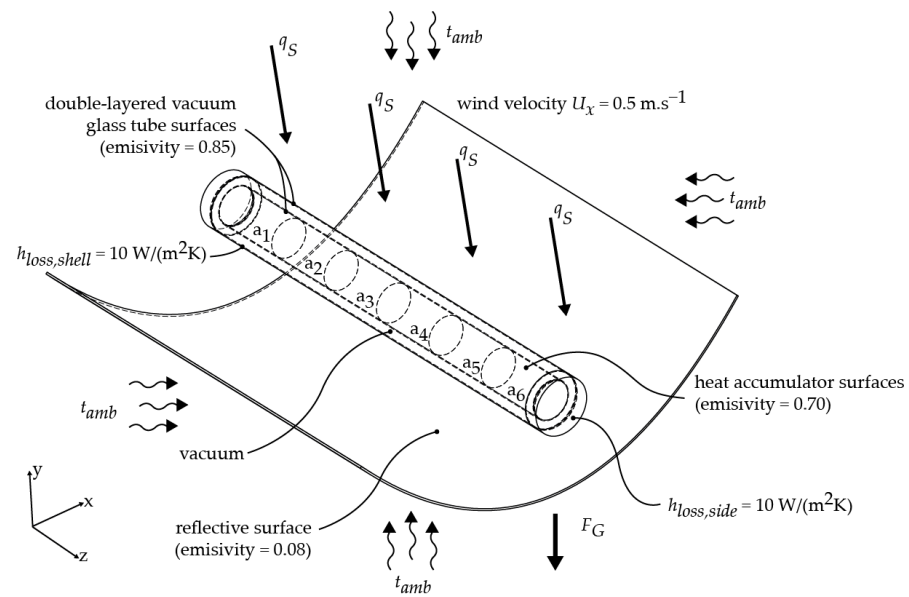


**Figure 4.** Basic layout and description of the calculation model.

The basic part of the model is heat accumulation blocks made of gray cast iron of a cylindrical shape with a diameter of 100 mm and a length of 200 mm (marked as  $a_1$  to  $a_6$ ). The model contains six pieces of heat accumulators, which were placed in a double-layered borosilicate vacuum tube, when a vacuum was defined between the layers, serving as thermal insulation. The thickness of the glass is 2 mm, the gap between the layers is 20 mm. The length of the tube corresponds to the length of the six heat accumulators and the length of the edge fillet, i.e., 1224 mm. At both ends, thermal insulating blocks are closing the heat accumulators inside the vacuum glass tube, their thickness is 40 mm and they exactly copy the shape of the end of the tube. The last part is a concentration-reflective element in the shape of a parabola with a width of 1100 mm, a total length of 1200 mm. The focal point at which the assembly of heat accumulators, glass vacuum tube, and insulators are located is 250 mm from the top of the parabola. Boundary conditions (BC) and computational domain are depicted in Figure 5.

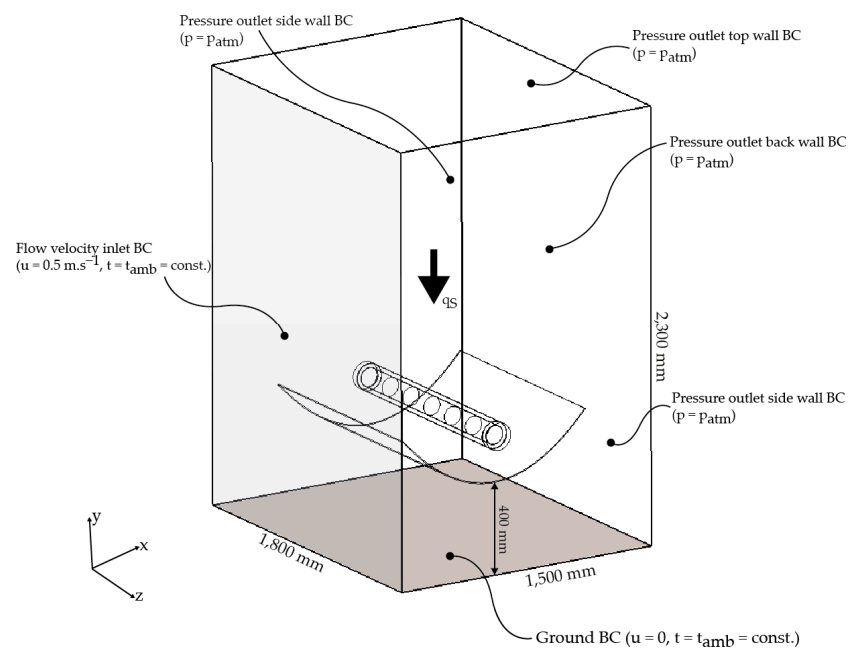


**Figure 5.** Computational domain and boundary conditions (BC).

In modeling, heat losses of  $10 \text{ W}/(\text{m}^2\text{K})$  from the outer shell and sides of the tube were considered. The airflow was set in the x-axis direction at  $0.5 \text{ m/s}$ . Ambient temperature, intensity, and angle of incidence of solar radiation were modeled based on a specific geographical location. Table 1 summarizes other material, physical and thermal properties of each part of the model. Numerical CFD analysis of the monitored parameters was carried out in Solidworks Flow Simulation version 2017 software (published by Dassault Systemes). The Discrete Ordinates radiation model was used to simulate solar heating, which also includes the absorption of thermal radiation by solids, due to the simple situation from the point of view of the medium flow in the model without expecting the formation of significant turbulent regions; the standard k- $\epsilon$  turbulence model was used. A module for monitoring the intensity of solar radiation based on latitude, day number of the year, and time was also used. This computing apparatus is long and extensively used [45–47].

**Table 1.** Material, physical and thermal properties of each part of the model.

	Material	Density [ $\text{kg}/\text{m}^3$ ]	Total Weight [kg]	Thermal Conductivity [ $\text{W}/(\text{mK})$ ]	Specific Heat Capacity [ $\text{J}/(\text{kgK})$ ]
Heat accumulator	Cast iron	7200	67.86	52	460
Vacuum glass tube	Borosilicate glass	2200	4.232	1.4	670
Concentration- reflective parabola	Polished aluminum foil	2700	0.120	237	900
Thermal isolation block	Mineral glass wool	130	0.156	0.035	1030

In fluid regions, SOLIDWORKS Flow Simulation solves the Navier–Stokes equations, which are formulations of mass, momentum and energy conservation laws:

$$\frac{\partial \rho}{\partial t} + \frac{\partial(\rho u_i)}{\partial x_i} = 0 \quad (1)$$

$$\frac{\partial(\rho u_i)}{\partial t} + \frac{\partial}{\partial x_j}(\rho u_i u_j) + \frac{\partial p}{\partial x_i} = \frac{\partial}{\partial x_j}(\tau_{ij} + \tau_{ij}^R) + S_i \quad (2)$$

$$\frac{\partial \rho H}{\partial t} + \frac{\partial \rho u_i H}{\partial x_i} = \frac{\partial}{\partial x_i} \left( u_j (\tau_{ij} + \tau_{ij}^R) + q_i \right) + \frac{\partial p}{\partial t} - \tau_{ij}^R \frac{\partial u_i}{\partial x_j} + \rho \epsilon + S_i u_i + Q_H \quad (3)$$

where  $u$  is fluid velocity,  $\rho$  is density,  $S_i$  is the mass-distributed external force (gravity or forces of rotation),  $H = h + u^2/2$ ,  $h$  is enthalpy,  $Q_H$  is the heat source per unit volume,  $\tau_{ij}$  is viscous stress tensor,  $\tau_{ij}^R$  is Reynolds viscous stress tensor, and  $q_i$  is diffusive heat flux. Indices indicate the summation in three coordinate directions. Heat transfer in solids and fluids with energy exchange between them (conjugate heat transfer) is an essential and implicit element of CAD-embedded CFD software. The phenomenon of heat conduction in solid media is described by the following equation:

$$\frac{\partial \rho e}{\partial t} = \frac{\partial}{\partial x_i} \left( \lambda_i \frac{\partial T}{\partial x_i} \right) + Q_H \quad (4)$$

where  $e$  is the specific internal energy,  $Q_H$  is specific heat release (or absorption) rate per unit volume and  $\lambda_i$  are the eigenvalues of the thermal conductivity tensor. In the Discrete Ordinates model, the whole  $4\pi$  directional domain at any location within the computational domain is discretized into the specified number of equal solid angles. A radiation governing equation can be written as follows:

$$\frac{dI(\vec{s}, \vec{r})}{ds} = -(\kappa + \sigma_s) \cdot I(\vec{s}, \vec{r}) + \kappa \cdot n^2 \cdot I_b(\vec{r}) + \frac{\sigma_s}{4\pi} \int_0^{4\pi} \phi(\vec{s}', \vec{s}) \cdot I(\vec{s}', \vec{r}) \cdot d\Omega' \quad (5)$$

where  $\vec{r}$  is position vector,  $\vec{s}$  is direction vector,  $\vec{s}'$  is scattering direction vector,  $s$  is path length,  $\kappa$  is absorption coefficient,  $n$  is refractive index,  $I_b$  is black body radiation intensity,  $\sigma_s$  is scattering coefficient,  $I$  is radiation intensity, which depends on position ( $\vec{r}$ ) and ( $\vec{s}$ ),  $\phi$  is phase function,  $\Omega'$  is solid angle. A more detailed description can be found in the supplied technical documentation [48].

The concentrated solar heater model for segmented heat accumulators was transformed into a computational mesh for simulation purposes. The Solidworks Flow Simulations software uses a unique mesh creating methodology, which consists of using immersed-body mesh. With this approach, the creation of a mesh begins independently of the geometry itself, and each mesh cell can arbitrarily intersect the boundary between solid and liquid. This allows using Cartesian-based mesh. Such a mesh can be defined as a set of cuboids (rectangular cells) that are adjacent to each other and to the outer boundary of the computational space and at the same time are oriented along with Cartesian coordinates. These cells can be divided into solid cells, fluid cells, and partial cells (cells intersected the immersed boundary). On partial cells, which intersect the surface separating the solid and fluid region, the two-scale wall function is then applied, which consists of two methods for thin boundary layer treatment or thick boundary layer treatment. This approach at the fluid/solid interface allows the solution of Navier–Stokes equations in these defined volumes. A complete mathematical apparatus for grid formation methods is provided in the available technical documentation of the software [49]. The result of this procedure was a computational mesh that had 876,294 cells, of which 659,257 were fluid cells and 217,037 solid cells.

The quality of the mesh and its effect on the result was tested using the grid-independent study, in which the gradual development of the parameter of the average temperature of heat accumulators was monitored depending on the change of the quality of the mesh, respective to the number of cells. The results of the grid-independent study are shown in Figure 6, where the stabilization of the monitored value at the level of approximately 875,000 cells can be seen; the overall mesh in section-view is depicted in Figure 7.

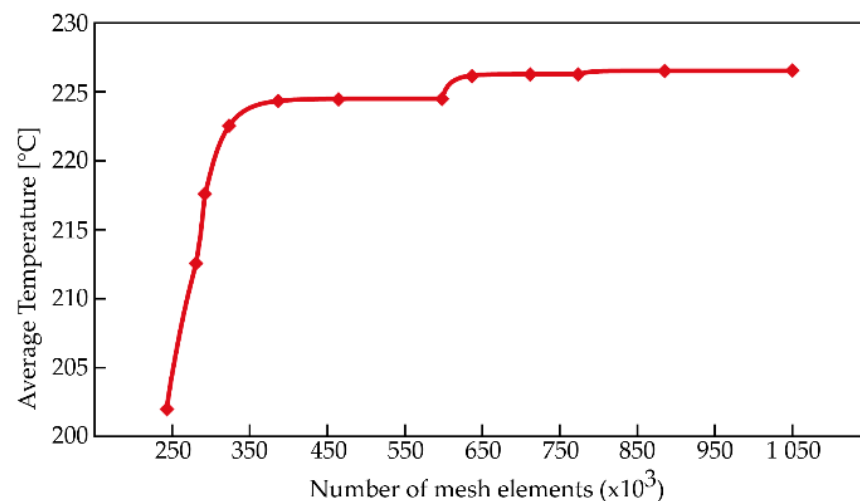


**Figure 6.** Results of the grid-independent study.

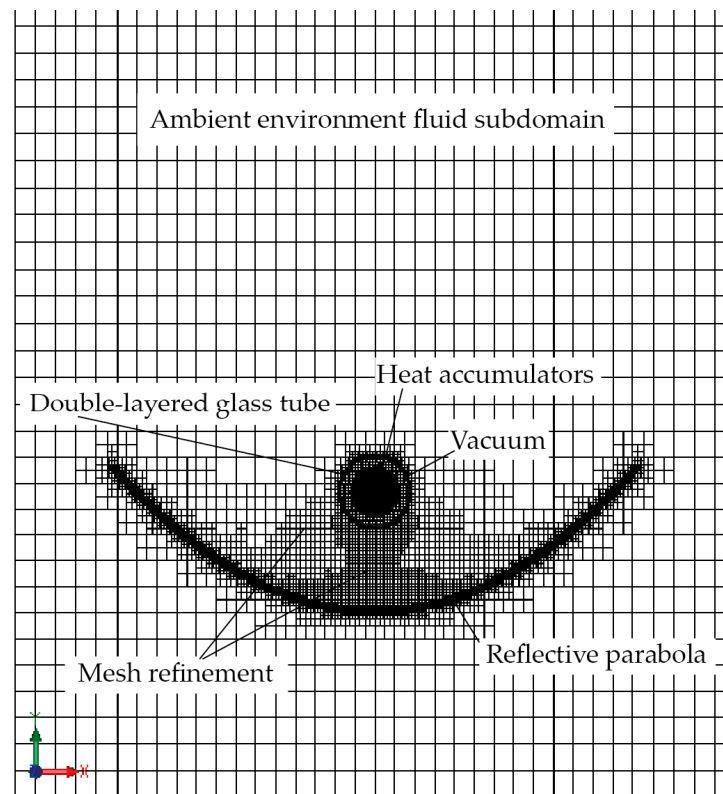


Figure 7. Section-view of meshed model.

### 3. Results

The evaluation of the presented design was carried out using transient simulations of the selected operation cases. For better evaluation of operating parameters, three geographical locations were selected, which represent different conditions in terms of solar intensity and ambient temperature, but at the same time, all three represent areas culturally suitable for implementing the proposed food preparation method. These areas are North Africa, South China, and Indonesia. From the point of view of solar radiation intensity, these areas were selected to cover the southern parts of the northern hemisphere in the range from  $33^{\circ}$  N, through the Tropic of Cancer, i.e.,  $23.5^{\circ}$  N to  $1^{\circ}$  N, where suitable climatic and insolation conditions can be expected for the operation of the proposed device. These regions will hereinafter be referred to as regions A, B, and C. The reference date was chosen on June 21 and simulations followed the entire 24-h period. For a combination of location B ( $23.5^{\circ}$  N), date June 21, and time 12:00, we obtained the ideal combination when the sun was directly above the concentrator and thus the device was attacked by the maximum intensity of solar radiation. It should be emphasized that in the simulations, static operation of the proposed concentrator was considered without gradual positioning of the device with respect to the changing position of the sun in the sky. In real operation, it is assumed that the device will be gradually positioned at approximately 30-min intervals.

The results of the analysis presented in Table 2 show the average temperature of all heat accumulation elements and the temperature of the outer surface of the vacuum glass tube at 12:00. The presented values quantified the expected results, i.e., the highest average temperature of the six heat accumulators, is reached by the device in locality B, followed by localities A and C. These results copy the angle of incidence of solar radiation and its intensity, respectively. For locality A, a maximum intensity value of  $1030 \text{ W/m}^2$  was calculated, for locality B it is  $1045 \text{ W/m}^2$  and for locality C it is  $960 \text{ W/m}^2$ .

**Table 2.** Average temperature of the heat accumulators and outer surface of the vacuum glass tube at 12:00.

	<b>The Maximum Intensity of Solar Radiation [W/m<sup>2</sup>]</b>	<b>Ambient Temperature [°C]</b>	<b>Latitude</b>	<b>The Average Temperature of the Heat Accumulators [°C]</b>	<b>The Average OuterSurface Temperature of the Vacuum Glass Tube [°C]</b>
Locality A (North Africa)	1030	25.1	33° N	206.83	94.55
Locality B (South China)	1045	25.6	23.5° N	227.23	106.29
Locality C (Indonesia)	960	25.9	1° N	137.65	62.99

Figure 8 shows the temperature field in the longitudinal section view of the device and a detailed view of the top and bottom of the model. The figure shows that the six heat accumulators do not reach the same temperature, while the heat accumulators that are located at the ends of the vacuum glass tube are most affected by heat loss through the heat insulation block. At higher temperatures (Figure 8A,B) the temperature stratification is more pronounced, with the highest temperature being in the middle of the device. At lower temperatures, this temperature stratification is less pronounced. A closer look at the top and bottom of the device shows the apparent heat transfer through conduction from the inner layer of the glass tube through the rounding to the outer layer, as well as the heat transfer by radiation from the cast iron heat accumulators. For better mutual comparison, all cases are visualized in the same color spectrum and using the same scale.

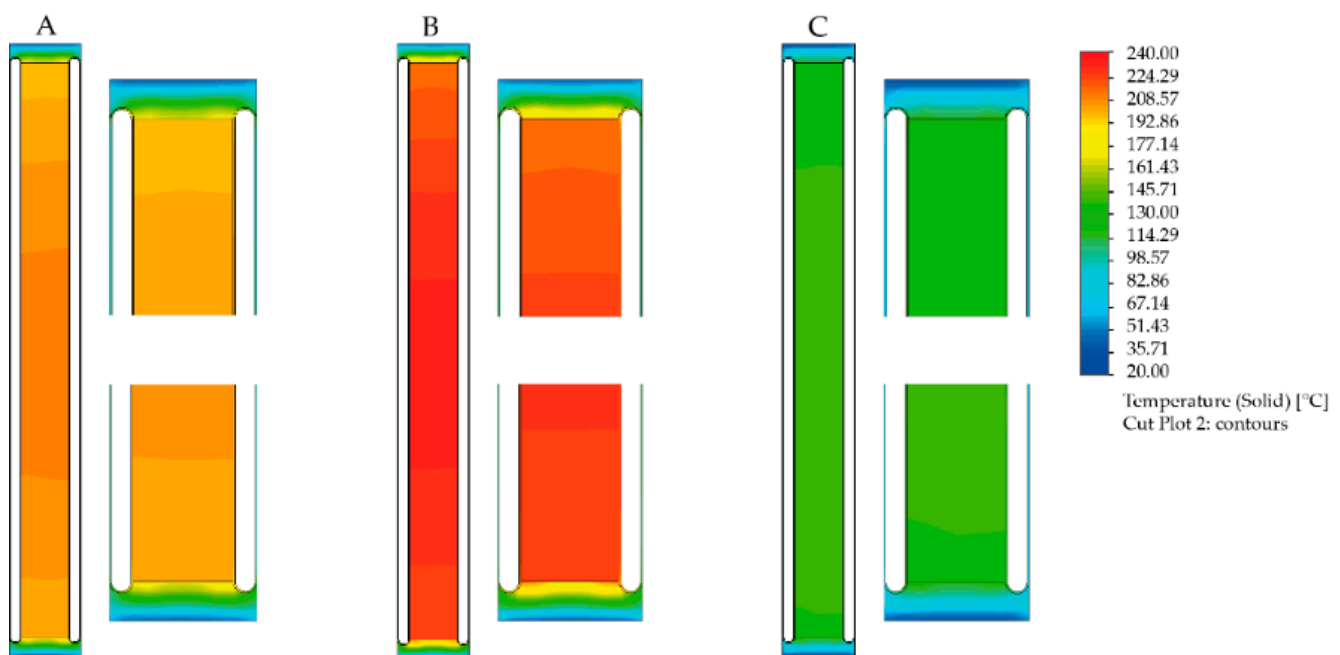


**Figure 8.** Temperature field in the longitudinal section view of the device and a detailed view of the top and bottom of the model for the North Africa (A), South China (B) and Indonesia (C).

A much more interesting result was obtained by comparing the average surface temperature of the outer layer of the vacuum glass tube, which in the case of sites A and B oscillates around 100 °C. The reason for this high temperature is the mentioned radiation of cast iron cylinders, which reach a temperature of over 200 °C, as well as heat transfer by conduction from the inner layer (which is in direct contact with the heat accumulators) through rounding to the outer layer.

From Figure 9, where the heat accumulators are shown in an isometric view, in addition to the temperature distribution, it is also possible to see the temperature non-uniformity in the Z-axis and the Y-axis. From the point of view of the Y-axis, a higher temperature can be seen in the lower part, which is caused by a higher heat flux of the reflected solar radiation from the parabolic concentrator (this fact is best visible in the case of location B).

Two scenarios were simulated in the next phase of the analysis. The first focused on a 24-h period in which the device was not positioned depending on the direction of the sun's rays and the heat accumulators were not removed. It is therefore a simulation of operation, where only the accumulation of thermal energy occurs without the direct input of the operator. Figure 10 shows the time course of the change in the average temperature of all heat accumulators (solid line) as well as the intensity of the solar radiation (dashed line) for each of the three locations.

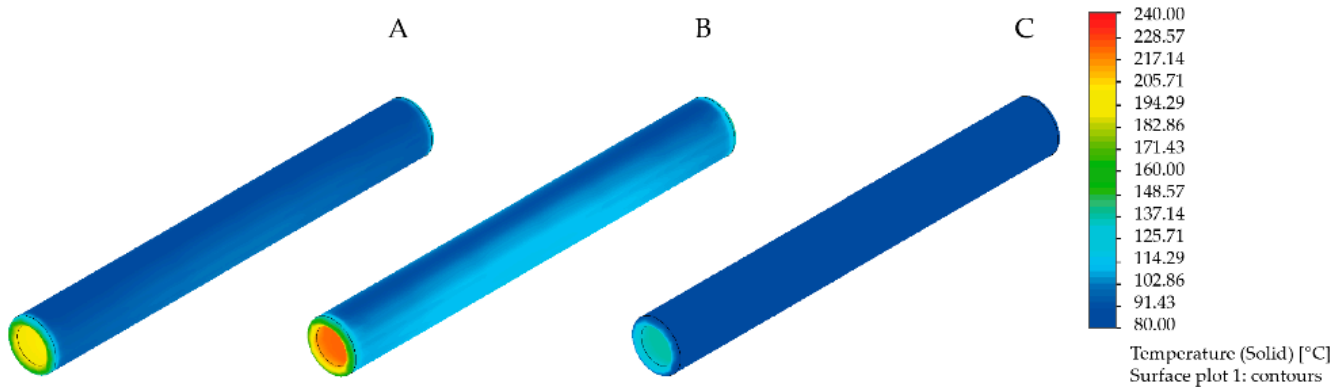


**Figure 9.** Isometric view of the surface temperature of the vacuum glass tube for the North Africa (A), South China (B) and Indonesia (C).

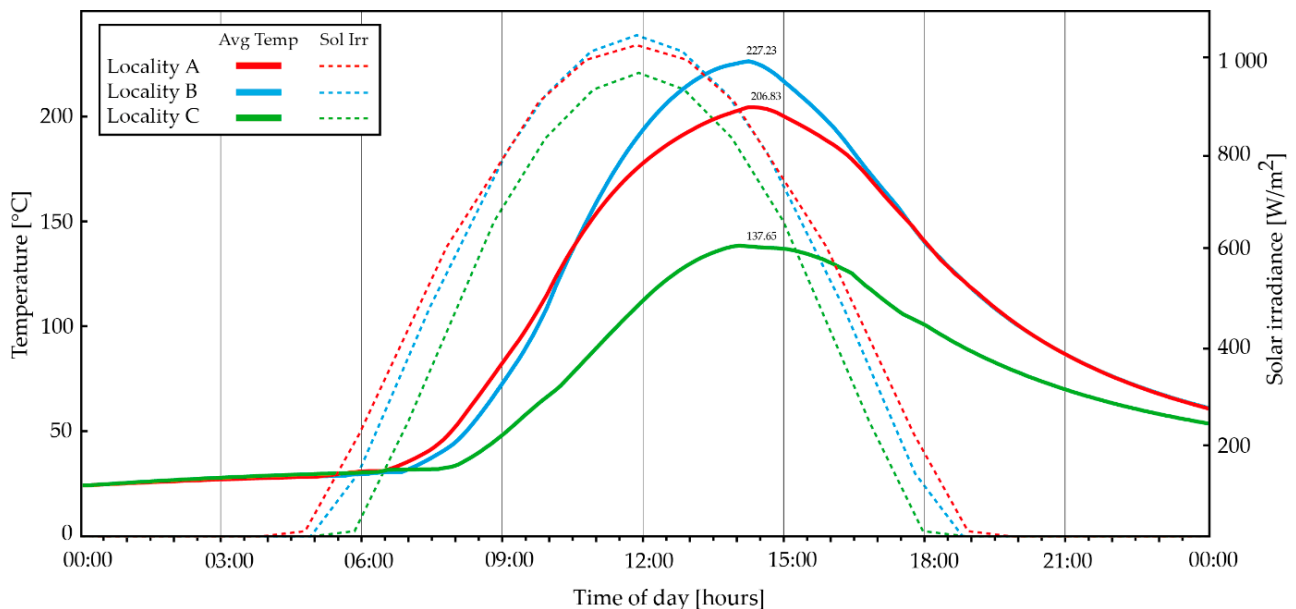


**Figure 10.** Time course of the change in the average temperature of heat accumulators and intensity of the solar radiation.

The picture shows that the device starts working, i.e., the temperature of the heat accumulators starts to increase from approximately 6:30, reaches its maximum value by approximately 14:30, then the temperature starts to decrease. All three geographical locations show approximately the same course, differing only in the reached temperature maximum. Also, due to the thermal insulation (the vacuum in the glass interlayer), the temperature does not drop below the initial temperature. However, it should be emphasized that such a simulated method of operation cannot be expected in real situations, where sequential rotation of the device by the operator during the heat storage process as well as gradual or complete removal of heat storage elements is expected. By sequentially positioning the device depending on the position of the sun in the sky, the device would reach its maximum temperature in the earlier hours of the day. However, the results of this simulation demonstrate the overall functionality of the device even in operating conditions, which bring non-ideal insolation conditions.

#### 4. Discussion

The above results demonstrated the functionality of the device in its basic form of operation, i.e., by charging all six heat accumulators from the same temperature. Further simulations considered the state in which the device is supplemented with discharged heat

accumulators, while in the device are heat accumulators in the charging process. Two situations were considered, Case 1, when the heat accumulators 3, 4, 5, and 6 are in the device and the charging process takes place, and later heat accumulators 1 and 2 that are in ambient temperature are subsequently added to the device. In Case 2, when the heat accumulators 5 and 6 are in the device and the charging process takes place, heat accumulators 1, 2, 3, and 4 that are in ambient temperature are subsequently added to the device.

The purpose of simulating this situation is to verify the assumed real-life operating scenarios of the proposed concentrated solar heater, in which the user would use only a part of the charged heat accumulators or gradually replenish the accumulators in the device. In these situations, it was necessary to consider the thermal inertia of individual heat accumulators resulting from the value of their specific heat capacity, as well as the coefficient of heat conduction, respectively transferred between the accumulators. This fact is especially important in the initial moments after the replenishment of discharged heat accumulators, which partially reduce the temperature charged accumulators in the device due to heat transfer, in accordance with the second law of thermodynamics.

In dealing with this situation, only locality B, date 21 June and the time 10:30, when the added heat accumulators begin to heat up, were considered. The simulation followed a period of sixteen hours. In the beginning, it was necessary to determine the current temperature of two and four heat accumulators at a time of 10:30, respectively. The simulation result shown in Figure 11 shows the temperature field in the longitudinal section view of the device. For Case 1, the average temperature of the heat storage elements is 201.51 °C, for Case 2 it is 182.84 °C. The figure shows, among other things, the internal volume of the glass tube, which in these cases is filled with air. The temperature map shows its relatively high temperature, which is visibly inhomogeneous due to convective flow.

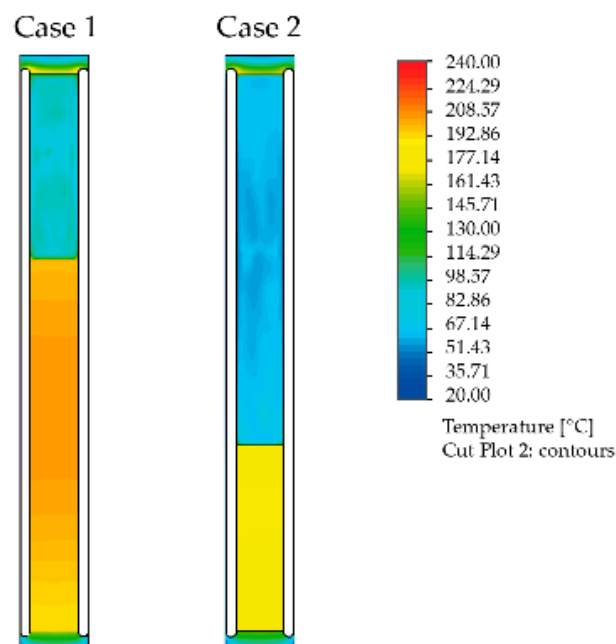


**Figure 11.** Temperature field in the longitudinal section view of the device with two and four heat accumulators at a time of 10:30, respectively (Case 1–device with four heat accumulators, Case 2–device with two heat accumulators).

The temperatures determined in this way formed the input to the simulation of charging the added heat accumulators. The simulation of charging two or four discharged heat accumulators was also divided into Case 1 and Case 2. In Case 1, two discharged heat accumulators were added to the device, in Case 2 we added four discharged heat accumulators into the simulation. Figures 12 and 13 show the temperature field in the section of a concentrated

solar heater, where the change in temperature of individual heat accumulators can be seen. The figures show the first hour of charging. Over time, it is clear to see a decrease in the temperature of the heat accumulators that were in the device, and thus initially had a higher temperature, as well as a further increase in replenished heat accumulators, both due to heat transfer from charged heat accumulators and also due to solar radiation.

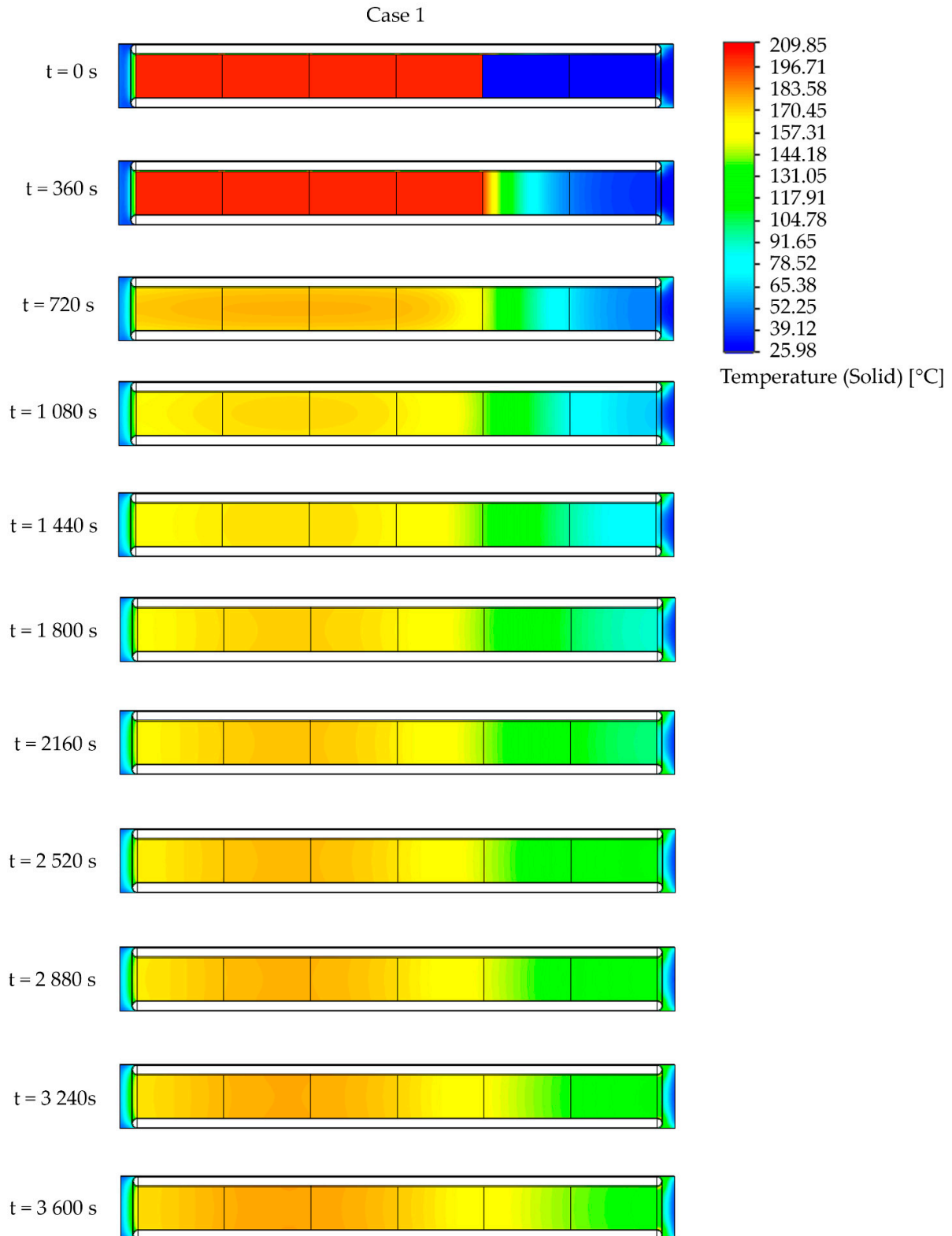


**Figure 12.** Temperature field in the longitudinal section view of heat accumulator in process of charging in Case 1.

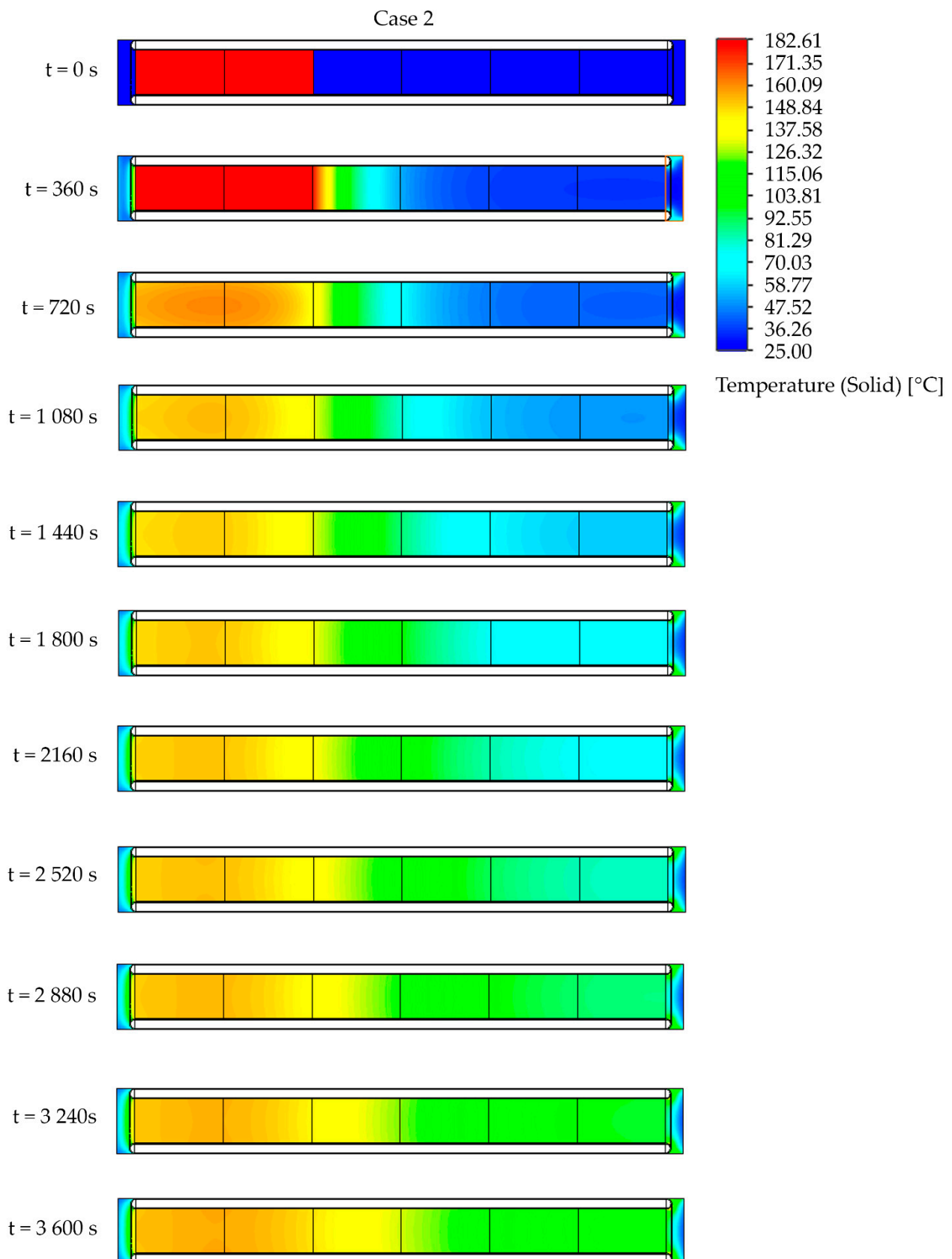


**Figure 13.** Temperature field in the longitudinal section view of heat accumulator in process of charging in Case 2.

Time course of the whole simulation is shown in Figure 14, where Case 1 on the left and Case 2 on the right can be seen. In both cases there are visible initial temperature decreases of charging heat accumulators; in Case 1, heat accumulator number 3 drops to the temperature of 154.1 °C, in Case 2 heat accumulator number 5 drops to the temperature of 142.8 °C. This decrease is caused by the heat conduction into the added heat accumulators (especially the adjacent ones). With increasing time, it is possible to observe the gradual heating of the added heat accumulators, while there is no longer heat removal from the originally charged heat accumulators, but heating caused by the solar radiation. During the entire heating period, the temperatures of the heat accumulators do not significantly match, with the largest difference occurring at the time of maximum temperature, being 23.7 °C for Case 01 and 25.8 °C for Case 2. The temperature of the heat accumulators only equalizes when they fall below 100 °C.

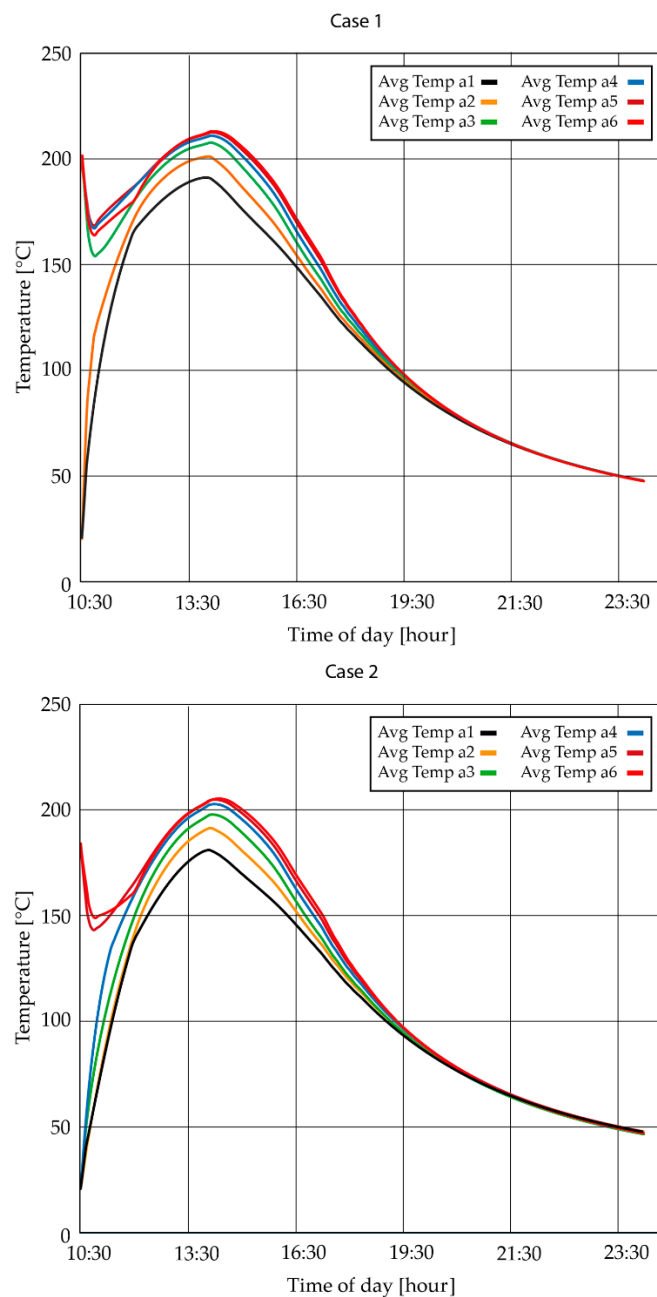


Figure 14. The course of the temperature of heat accumulators for Case 1 and Case 2.

The usability of the proposed device was finally assessed by calorimetric analysis of accumulated heat. This analysis assumes the need to exceed a certain temperature of the prepared food; this increase in temperature is provided by the heat accumulators, with which the food is in contact and there is heat exchange between them in terms of the second law of thermodynamics. The resulting temperature of the heat accumulator/food system can be determined using a calorimetric equation (Equations (6) and (7)) [50].

$$m_a \cdot c_a \cdot (t_a - t) = (m_F \cdot c_F \cdot (t - t_F)) \quad (6)$$

$$t = \frac{(m_a \cdot c_a \cdot t_a) + (m_F \cdot c_F \cdot t_F)}{m_a \cdot c_a + m_F \cdot c_F} \quad (7)$$

where  $m$  is the weight,  $c$  is the specific heat capacity and  $t$  is the temperature. Index  $a$  applies to quantities and values related to the heat accumulators,  $F$  to food. The resulting temperature of heat accumulators/food system is denoted as  $t$ . This analysis was based on known parameters of the proposed device, i.e., six heat accumulators made of gray cast iron (specific heat capacity 460 J/(kg.K) and a total weight of 67.86 kg) and properties of the prepared food, which in this case is represented with chicken meat (specific heat capacity 3100 J/(kg.K) and a total weight of 3.5 kg). Using Equation (2), the resulting temperature is 175 °C, which is 10 °C higher than the so-called pasteurization temperature required for chicken meat. Thanks to the thermal insulation of the food preparation site with a layer of soil cover, it is then possible to assume longer maintenance of the required temperature using the slow cooking method of food preparation.

The overall analysis of the results pointed to three areas of design that need to be addressed accordingly. The first area concerns the effort to eliminate the increased temperature of the outer surface of the glass vacuum tube. The achieved temperatures at the highest performances may pose a threat to the health of the operator of this equipment in careless handling. If we consider the heat transfer in the earth oven from the heat accumulators to the food through heat transfer by conduction and convection, then we would be able to eliminate this increased temperature of the outer glass vacuum tube by the selective coating of cast iron cylinders, thereby reducing the amount of radiation from their surface. The second area is the design of the chassis, which must not significantly cast a shadow on the concentration-reflective surface, which could reduce the overall performance of the device. In solving this problem, it is possible to build on existing technical wheel solutions with a low number of spokes. The third area concerns the proposal of further use of heat accumulators, which can be used for water heating and disinfection. At the achieved maximum temperatures of the heat accumulators, it is possible to reach water temperatures above 100 °C, with a water volume in the range of 8 L to 10 L. Here, however, it is necessary to change the approach from an earth oven, where water heating is out of the question, and propose the equipment enabling thermal connection of the vessel with water and heat accumulators. A possible solution could be a container with an increased heat exchange area through fins and with openings in the casing for accommodating heat accumulators. However, this issue will be addressed in the next phase of research.

## 5. Conclusions

The presented paper deals with the design and evaluation of the concept of a concentrated solar heater for segmented heat accumulators. The purpose of this design is to cover the energy needs of selected communities in terms of food preparation without the need to use fossil fuels, which have a negative impact in the form of extensive use of forests beyond their sustainability, endangerment of human health by combustion products, and accidents arising from the use of open flames. The proposed device is based on the traditional method of food preparation in the so-called earth oven; however, the fire-heated stones are replaced by heat accumulators heated by solar radiation. This procedure eliminates the need to change the usual and long-term methods of food preparation of selected communities. The device combines a parabolic concentrator, heat accumulators, and solar glass vacuum

tubes, which reduces heat loss and increases the performance of the device. For better evaluation of operating parameters, three geographical locations were selected, which represent different conditions in terms of solar intensity and ambient temperature, but at the same time, all three represent areas culturally suitable for implementing the proposed food preparation method. These areas are North Africa, South China, and Indonesia. From the point of view of solar radiation intensity, these areas were selected to cover the southern parts of the northern hemisphere in the range from 33 °N, through the Tropic of Cancer, i.e., 23.5° N to 1° N, where suitable climatic and insolation conditions can be expected for the operation of the proposed device. The results showed an increase in the temperature of the heat accumulators up to 206.83 °C; 227.23 °C and 137.65 °C for each of the locations. In terms of time, the heat accumulators reached their maximum temperature in about eight hours, but without the active approach of the operator to position the entire device in terms of the movement of the sun in the sky, which would significantly shorten this time. Based on a calorimetric analysis of the system, which consists of food and heat accumulators, it was found that the resulting temperature exceeds 175 °C, which ensures the so-called pasteurization temperature necessary for safe and healthy food preparation. The results of simulations demonstrate the overall functionality of the device, even in operating conditions, which bring non-ideal insolation conditions.

**Author Contributions:** Conceptualization, M.B. and R.R.; methodology, M.B.; validation, J.R.; formal analysis, M.B.; resources, R.R.; data curation, M.B., A.S., V.F.; writing—original draft preparation, M.B.; writing—review and editing, M.B., A.S.; visualization, M.B.; supervision, R.R. All authors have read and agreed to the published version of the manuscript.

**Funding:** This paper was created in connection with the project VEGA 1/0290/21 Study of the behavior of heterogeneous structures based on PCM and metal foams as heat accumulators with application potential in technologies for obtaining and processing earth resources. This research was funded by the Scientific Grant Agency of the Ministry of Education, Science, Research and Sport of the Slovak Republic (VEGA). This paper was created in connection with the project 048TUKE-4/2021 Universal educational-competitive platform.

**Institutional Review Board Statement:** Not applicable.

**Informed Consent Statement:** Not applicable.

**Conflicts of Interest:** The authors declare no conflict of interest.

## References

1. Liu, W.; Hou, Y.; Liu, W.; Yang, M.; Yan, Y.; Peng, C.; Yu, Z. Global estimation of the climate change impact of logging residue utilization for biofuels. *For. Ecol. Manag.* **2020**, *462*, 118000. [[CrossRef](#)]
2. Wang, X.; Xu, L.; Cui, S.; Wang, C.-H. Reflections on coastal inundation, climate change impact, and adaptation in built environment: Progresses and constraints. *Adv. Clim. Chang. Res.* **2020**, *11*, 317–331. [[CrossRef](#)]
3. Zhao, X.; Huang, G.; Lu, C.; Zhou, X.; Li, Y. Impacts of climate change on photovoltaic energy potential: A case study of China. *Appl. Energy* **2020**, *280*, 115888. [[CrossRef](#)]
4. Yang, Y.C.E.; Son, K.; Hung, F.; Tidwell, V. Impact of climate change on adaptive management decisions in the face of water scarcity. *J. Hydrol.* **2020**, *588*, 125015. [[CrossRef](#)]
5. Macusi, E.D.; Macusi, E.S.; Jimenez, L.A.; Catam-isan, J.P. Climate change vulnerability and perceived impacts on small-scale fisheries in eastern Mindanao. *Ocean. Coast. Manag.* **2020**, *189*, 105143. [[CrossRef](#)]
6. Li, R.; Leung, G.C.K. The relationship between energy prices, economic growth and renewable energy consumption: Evidence from Europe. *Energy Rep.* **2021**, *7*, 1712–1719. [[CrossRef](#)]
7. Jun, W.; Mughal, N.; Zhao, J.; Shabbir, M.S.; Niedbała, G.; Jain, V.; Anwar, A. Does globalization matter for environmental degradation? Nexus among energy consumption, economic growth, and carbon dioxide emission. *Energy Policy* **2021**, *153*, 112230. [[CrossRef](#)]
8. Meng, J.; Hu, X.; Chen, P.; Coffman, D.; Han, M. The unequal contribution to global energy consumption along the supply chain. *J. Environ. Manag.* **2020**, *268*, 110701. [[CrossRef](#)] [[PubMed](#)]
9. Inchauspe, J.; Li, J.; Park, J. Seasonal patterns of global oil consumption: Implications for long term energy policy. *J. Policy Model.* **2020**, *42*, 536–556. [[CrossRef](#)]
10. BP Plc. *BP Statistical Review of World Energy 2020*; BP Plc: London, UK, 2020; pp. 8–11.

11. U.S. Energy Information Administration. *The Middle East, Africa, and Asia Now Drive Nearly All Global Energy Consumption Growth—International Energy Statistics 2020*; U.S. Energy Information Administration: Washington, DC, USA, 2020; pp. 1–10.
12. U.S. Energy Information Administration. *International Energy Outlook 2020 (IEO2020)*; U.S. Energy Information Administration: Washington, DC, USA, 2020; pp. 1–7.
13. Cehlár, M.; Teplická, K.; Seňová, A. Risk management as instrument for financing projects in mining industry. In Proceedings of the 11th International Multidisciplinary Scientific Geoconference and EXPO—Modern Management of Mine Producing, Geology and Environmental Protection, SGEM 2011, Varna, Bulgaria, 20–25 June 2011; Volume 1, pp. 913–920.
14. Hrehová, D.; Cehlár, M.; Rybár, R.; Mitterpachová, N. Mining technology with drilling-blasting operations. In Proceedings of the 12th International Multidisciplinary Scientific GeoConference and EXPO—Modern Management of Mine Producing, Geology and Environmental Protection, SGEM 2012, Varna, Bulgaria, 17–23 June 2012; Volume 1, pp. 675–682.
15. Batchelor, S.; Talukder, M.A.R.; Uddin, M.R.; Mondal, S.K.; Islam, S.; Redoy, R.K.; Hanlin, R.; Khan, M.R. Solar e-Cooking: A Proposition for Solar Home System Integrated Clean Cooking. *Energies* **2018**, *11*, 2933. [[CrossRef](#)]
16. Cravioto, J.; Ohgaki, H.; Che, H.S.; Tan, C.; Kobayashi, S.; Toe, H.; Long, B.; Oudaya, E.; Rahim, N.A.; Farzaneh, H. The Effects of Rural Electrification on Quality of Life: A Southeast Asian Perspective. *Energies* **2020**, *13*, 2410. [[CrossRef](#)]
17. World Health Organization. *Burning Opportunity: Clean Household Energy for Health, Sustainable development, and Wellbeing of Women and Child*; World Health Organization: Geneva, Switzerland, 2016; p. 9.
18. Malla, S.; Timilsina, G.R. *Household Cooking Fuel Choice and Adoption of Improved Cookstoves in Developing Countries*; The World Bank Development Research Group: Washington, DC, USA, 2014.
19. Anwar, M.A.; Nasreen, S.; Tiwari, A.K. Forestation, renewable energy and environmental quality: Empirical evidence from Belt and Road Initiative economies. *J. Environ. Manag.* **2021**, *291*, 112684. [[CrossRef](#)] [[PubMed](#)]
20. Manolis, E.N.; Zagas, T.D.; Karetos, G.K.; Poravou, C.A. Ecological restrictions in forest biomass extraction for a sustainable renewable energy production. *Renew. Sustain. Energy Rev.* **2019**, *110*, 290–297. [[CrossRef](#)]
21. Galik, C.S.; Benedum, M.E.; Kauffman, M.; Becker, D.R. Opportunities and barriers to forest biomass energy: A case study of four U.S. states. *Biomass Bioenergy* **2021**, *148*, 106035. [[CrossRef](#)]
22. Balmes, J.R. Household air pollution from domestic combustion of solid fuels and health. *J. Allergy Clin. Immunol.* **2019**, *143*, 1979–1987. [[CrossRef](#)]
23. Li, Y.; Xu, H.; Wang, J.; Hang Ho, S.S.; He, K.; Shen, Z.; Ning, Z.; Sun, J.; Li, L.; Lei, R.; et al. Personal exposure to PM<sub>2.5</sub>-bound organic species from domestic solid fuel combustion in rural Guanzhong Basin, China: Characteristics and health implication. *Chemosphere* **2019**, *227*, 53–62. [[CrossRef](#)] [[PubMed](#)]
24. Wang, D.; Li, Q.; Shen, G.; Deng, J.; Zhou, W.; Hao, J.; Jiang, J. Significant ultrafine particle emissions from residential solid fuel combustion. *Sci. Total. Environ.* **2020**, *715*, 136992. [[CrossRef](#)]
25. Du, W.; Yun, X.; Fu, N.; Qi, M.; Wang, W.; Wang, L.; Chen, Y.; Shen, G. Variation of indoor and outdoor carbonaceous aerosols in rural homes with strong internal solid fuel combustion sources. *Atmos. Pollut. Res.* **2020**, *11*, 992–999. [[CrossRef](#)]
26. Ezzati, M.; Kammen, D.M. The Health Impacts of Exposure to Indoor Air Pollution from Solid Fuels in Developing Countries: Knowledge, Gaps, and Data Needs. *Environ. Health Perspect.* **2002**, *110*, 1057–1068. [[CrossRef](#)]
27. Ray, I.; Smith, K.R. Towards safe drinking water and clean cooking for all. *Lancet Glob. Health* **2021**, *9*, 361–365. [[CrossRef](#)]
28. Quinn, A.K.; Bruce, N.; Puzzolo, E.; Dickinson, K.; Sturke, R.; Jack, D.W.; Mehta, S.; Shankar, A.; Sherr, K.; Rosenthal, J.P. An analysis of efforts to scale up clean household energy for cooking around the world. *Energy Sustain. Dev.* **2018**, *46*, 1–10. [[CrossRef](#)]
29. Rosenthal, J.; Quinn, A.; Grieshop, A.P.; Pillarisetti, A.; Glass, R.I. Clean cooking and the SDGs: Integrated analytical approaches to guide energy interventions for health and environment goals. *Energy Sustain. Dev.* **2018**, *42*, 152–159. [[CrossRef](#)]
30. Neto-Bradley, A.P.; Rangarajan, R.; Choudhary, R.; Bazaz, A. A clustering approach to clean cooking transition pathways for low-income households in Bangalore. *Sustain. Cities Soc.* **2021**, *66*, 102697. [[CrossRef](#)]
31. Aemro, Y.B.; Moura, P.; de Almeida, A.T. Experimental evaluation of electric clean cooking options for rural areas of developing countries. *Sustain. Energy Technol. Assess.* **2021**, *43*, 100954.
32. Kajumba, P.K.; Okello, D.; Nyeinga, K.; Nydal, O.J. Experimental investigation of a cooking unit integrated with thermal energy storage system. *J. Energy Storage* **2020**, *32*, 101949. [[CrossRef](#)]
33. Solar Cooker Distribution—S.C.I. Available online: <http://www.solarcookers.org/our-work/solar-cooker-distribution/> (accessed on 3 June 2020).
34. Arunachala, U.C.; Kundapur, A. Cost-effective solar cookers: A global review. *Sol. Energy* **2020**, *207*, 903–916. [[CrossRef](#)]
35. Rodríguez Morales, J.Á.; González-Avilés, M.; Servín Campuzano, H.; Maserá, O. T’imani a Multifunctional Solar System to Provide Cooking and Water Heating Rural Energy Needs. *Energies* **2020**, *13*, 3429. [[CrossRef](#)]
36. Zafar, H.A.; Badar, A.W.; Butt, F.S.; Khan, M.Y.; Siddiqui, M.S. Numerical modeling and parametric study of an innovative solar oven. *Sol. Energy* **2019**, *87*, 411–426. [[CrossRef](#)]
37. Ayub, I.; Nasir, M.S.; Liu, Y.; Munir, A.; Yang, F.; Zhang, Z. Performance improvement of solar bakery unit by integrating with metal hydride based solar thermal energy storage reactor. *Renew. Energy* **2020**, *161*, 1011–1024. [[CrossRef](#)]
38. Bhave, A.G.; Kale, C.K. Development of a thermal storage type solar cooker for high temperature cooking using solar salt. *Sol. Energy Mater. Sol. Cells* **2020**, *208*, 110394. [[CrossRef](#)]
39. Kumaresan, G.; Santosh, R.; Raju, G.; Velraj, R. Experimental and numerical investigation of solar flat plate cooking unit for domestic applications. *Energy* **2018**, *157*, 436–447. [[CrossRef](#)]

40. Sagade, A.A.; Samdarshi, S.K.; Lahkar, P.J.; Sagade, N.A. Experimental determination of the thermal performance of a solar box cooker with a modified cooking pot. *Renew. Energy* **2020**, *150*, 1001–1009. [[CrossRef](#)]
41. Mawire, A.; Lentswe, K.; Owusu, P.; Shobo, A.; Darkwa, J.; Calautit, J.; Worall, M. Performance comparison of two solar cooking storage pots combined with wonderbag slow cookers for off-sunshine cooking. *Sol. Energy* **2020**, *208*, 1166–1180. [[CrossRef](#)]
42. Chaudhary, R.; Yadav, A. Twin vessel solar cook stove for the simultaneous cooking of two different cooking articles. *Sol. Energy* **2020**, *208*, 688–696. [[CrossRef](#)]
43. Hosseinzadeh, M.; Faezian, A.; Mirzababae, S.M.; Zamani, H. Parametric analysis and optimization of a portable evacuated tube solar cooker. *Energy* **2020**, *197*, 116816. [[CrossRef](#)]
44. Radim Rybár, R.; Kudelas, D.; Beer, M.; Horodníková, J. Elimination of Thermal Bridges in the Construction of a Flat Low-Pressure Solar Collector by Means of a Vacuum Thermal Insulation Bushing. *J. Sol. Energy Eng.* **2015**, *137*, 054501. [[CrossRef](#)]
45. Iqbal, M. *An Introduction to Solar Radiation*; Academic Press: Toronto, ON, Canada, 1983; pp. 303–334.
46. Bird, R.E.; Hulstrom, R.L. *A Simplified Clear Sky Model for Direct and Diffuse Insolation on Horizontal Surface*; Solar Energy Research Institute: Golden, CO, USA, 1981; p. 46.
47. Badescu, V. *Modeling Solar Radiation at the Earth's Surface*; Springer: Berlin, Germany, 2008; pp. 93–113.
48. Dassault Systemes. *Solidworks Flow Simulations Technical Reference*; Dassault Systemes: Vélizy-Villacoublay, France, 2017.
49. Sobachkin, A.; Dumnov, G. *Numerical Basis of CAD-Embedded CFD*; Solidworks Technical Reference; Dassault Systemes: Vélizy-Villacoublay, France, 2017.
50. Cengel, Y.; Boles, M. *Thermodynamics: An Engineering Approach*, 8th ed.; McGraw-Hill Education: New York, NY, USA, 2014.